Ion channels in icosahedral virus: a comparative analysis of the structures and binding sites at their fivefold axes

Susana G. Kalko,[‡] Raul E. Cachau,[§] and Abelardo M. Silva*

*Instituto de Investigaciones Bioquimicas (INIBIBB), 8000 Bahia Blanca, Argentina; [‡]Departamento de Fisica Facultad de Ciencias Exactas, Universidad Nacional de La Plata, La Plata, Argentina; Structural Biochemistry Laboratory, Biomedical Supercomputer Center, PRI/Dyn Corp., and [§]National Cancer Institute, Frederick Cancer Research and Development Center, Frederick, Maryland 21702-1201

ABSTRACT An analysis of the crystallographically determined structures of the icosahedral protein coats of Tomato Bushy Stunt Virus, Southern Bean Mosaic Virus, Satellite Tobacco Necrosis Virus, Human Rhinovirus 14 and Mengovirus around their fivefold axes is presented. Accessibilities surfaces, electrostatic energy profile calculations, ion-protein interaction energy calculations, free energy perturbation methods and comparisons with structures of chelating agents are used in this study. It is concluded that the structures built around the viral fivefold axes would be adequate for ion binding and transport. Relative ion preferences are derived for the binding sites, using free energy perturbation methods, which are consistent with the experimental data when available. In the cases where crystallographic studies determined the existence of ions on the fivefold axes, our results indicate that they would correspond to ions in crystallization or purification buffers. The environment of the fivefold axes are rich in polar residues in all icosahedral viral structures whose atomic coordinates are available, including some that are not being analyzed in detail in this work. The fivefold channel-like structures have most of the basic properties expected for real ion channels including a funnel at the entrance, a polar internal environment with frequent alternation of acidic and basic residues, ion binding sites, the capability to induce ion dehydration and ion transit from the external viral surface to the binding sites.

INTRODUCTION

Protein ion channel structures remain elusive despite their importance for understanding fundamental physiological processes. The main obstacles for obtaining reliable high resolution atomic models of ion channels have been the difficulties in crystallizing membrane-bound proteins, thus inhibiting the use of x-ray crystallographic techniques on the problem. Nevertheless, some of their general properties have been deduced using a wide variety of methods. The general picture emerging indicates that channels like the GABA receptor, the Na channel or the Gly channel, are formed by the symmetric or quasi-symmetric association, around an axis, of homologous protein subunits. Also, the nicotinic acetylcholine receptor (AChR), an archetypical protein channel, displays quasi-fivefold symmetry. The channel walls are most likely lined by hydrophilic residues that would create a polar environment adequate for ion transport. An amino acid sequence analysis of the AChR superfamily of ligand-gated channels suggests that there might be a larger proportion of hydroxyl containing side chains in anionic than in cationic channel walls, (Stroud et al., 1990). This might indicate that the anion binding sites are built up by hydroxyl dipoles as observed, for example, in the sulfate-binding proteins (Pflugrath and Quiocho, 1988). Other models propose that the AChR channel would include planes, perpendicular to the channel axis, of alternating charges formed by fivefold related acidic and basic amino acids (Young et al., 1985). Those arrays of charges might act as focusing ion devices. There is evidence of the existence of a funnel shaped structure towards the extracellular membrane surface in the AChR (Stroud et al., 1990), although it is not clear whether its main function relates to capturing the ligand, the ions or both. There are several models for the energetics of the ion transport based on conductivity measurements. The ion-protein interaction energies derived have profiles with one or several minima along the channel axis. This might indicate the existence of ion binding sites within the channel (Cukierman et al., 1985) and that the ion transport might be seen as a succession of binding states. The mechanisms for ion dehydration, ion selectivity and gating are fundamental channel functions which are not well understood at the molecular level today and most likely will not be until a high resolution model of a protein ion channel is available.

Icosahedral viral protein coats provide by their very nature examples of highly symmetrical arrangements of protein subunits. The basic folding motif for the protein subunits seems to be the same for different icosahedral viruses: the antiparallel β-barrel. The variations on this universal theme are so numerous and complex that we no longer can envision the protein coat as just an envelope for the nucleic acid. Rather we have to consider that there might be functions of the capsid still to be discovered.

In an earlier work on the analysis of the structure of the small icosahedral plant virus Southern Bean Mosaic Virus (SBMV), we proposed that the structure of the fivefold related viral protein subunits could function as an ion channel, (Silva et al., 1987*a*). In the present work we attempt to establish whether this is a general property of icosahedral viruses. This would provide experimentally determined models for ion channels as well as new insights into viral physiology. In the following paper in this series, a part of the fivefold channel of Human Rhinovirus 14 is analyzed using energy minimization and molecular dynamics methods.

Address correspondence to Dr. Cachau.

0006-3495/92/10/1133/13 $2.00

There are several icosahedral viral particles whose structures have been determined by x-ray crystallographic techniques and therefore can be used to further explore the viral ion-channel hypothesis. In this paper we analyze the structures of Tomato Bushy Stunt Virus (TBSV) (Harrison et al., 1978; Olson et al., 1983), Satellite Tobacco Necrosis Virus (STNV) (Liljas et al., 1982; Jones et al., 1984), Human Rhinovirus 14 (HRV14) (Rossmann et al., 1985; Arnold et al., 1990) and Mengovirus (Luo et al., 1987; Krishnaswamy and Rossmann, 1990). It has been reported that some of these structures could function as ion channels at their fivefold axes, (Silva et al., 1987*a*; Eisenman et al., 1988*a*).

STNV is the simplest icosahedral virus of known structure. Its capsid is formed by 60 copies of an unique type of protein. According to the nomenclature of Caspar and Klug (1962), its triangulation number is $T = 1$. The protein subunits follow an exact icosahedral arrangement, Fig. 1. All 60 protein subunits are identical and they fold as a very simple β-barrel, Fig. 2 *a*.

TBSV and SBMV coat proteins are built up by 180 copies of subunits of the same type, so their triangulation number are defined as $T = 3$. The subunits, although having identical amino-acid sequences, are not all structurally equivalent since they have to accommodate different symmetry environments. That is, they have to pack either as pentamers or hexamers, Fig. 1, *b* and *c*. Then, three types of subunits can be distinguished. Subunits A form the pentamers around icosahedral fivefold axes, and pairs of subunits B and C form hexamers around icosahedral threefold axes. The coat proteins of TBSV and SBMV have an almost identical fold, Fig. 2, *b* and *c*.

HRV14 and Mengovirus are picornaviruses. All picornavirus protein coats are formed by 60 protomers icosahedrally arranged. Thus, their triangulation number is $T = 1$. In turn, each promoter is formed by four protein subunits, VP1, VP2, and VP3, which are on the external viral surface, and the small subunit VP4, which is totally internal. All three subunits VP1, VP2, and VP3 have a β-barrel folding similar to the $T = 3$ plant viruses SBMV and TBSV. Their radial position and orientation relative to the icosahedral symmetry axes are also homologous to those of the $T = 3$ plant viruses. Thus, the protein coat can be analyzed in terms of pentamers and hexamers with a pseudo $T = 3$ triangulation number, Fig. 1. Subunits VP1 are by the fivefold axes and VP2 and VP3 by the threefold axes creating the hexamers, Figs. 2, *d* and *e*.

Other icosahedral viruses whose structures have been determined are: the picornaviruses poliovirus (Hogle et al., 1985), foot-and-mouth disease virus (Acharya et al., 1989) and serotype 1A of Human Rhinovirus (Kim et al., 1989); Turnip Crinkle Virus (TCV) which is a $T = 3$ particle homologous to TBSV (Hogle et al., 1986); a $T = 1$ SBMV particle produced by in vitro assembly of SBMV subunits proteolyzed at their amino-terminal end (Erickson et al., 1985); Bean-Pod Mottle Virus (BPMV) which is a $T = 1$ particle although it can be interpreted as a pseudo $T = 3$ (Chen et al., 1989); the bacterial virus MS2 which has a $T = 3$ triangulation (Valegard et al., 1990); the insect virus Black Beetle virus which is a $T = 3$ particle (Hosur et al., 1987); Canine Parvovirus which displays a wide cylindrical structure at the fivefold axes (Tsao et al., 1991); Simian Virus 40 which shows a large inverted funnel pointing toward the outside, with a narrow section close to the surface (Liddington et al., 1991).

METHODS

Interaction energies were computed using the pair potentials derived by S. Fraga (Fraga et al., 1982; Bidacovich et al., 1990). To develop this potential, extensive and accurate self-consistent field calculations were first carried out for interaction between pairs of different type of molecules, like water, individual amino acids, purines, pyrimidines, ions, et cetera. The total energy was computed for a given pair of molecules at different relative orientation and separations. From the molecular energies for these associations and those for the individual molecules, a set of interaction energies was obtained (Clementi, 1980). These values were then fitted by a function expressed as a 1/R expansion with coefficients to be determined by the fitting. The intermolecular potential energy function includes coulombic, polarization, dispersion and repulsion terms. It has to be noticed that this pair potential approximation would be very inaccurate for some type of ions including Be and Mg (Corongiu and Clementi, 1978). Therefore, calculations involving those ions will not be performed.

The potential function was implemented within the protein conformation analysis package (PCAP) (Snow and Amzel, 1986; Cachau et al., 1990), that performs the molecular mechanics, molecular dynamics, electrostatic and free energy perturbation calculations. The electrostatic profiles are quite accurate since hydrogen atoms are explicitly included and an extended atom classification set (Nilar et al., 1984) is used. Also, the ab-initio and nonlocal nature of the fitting of this potential should allow its applicability to different systems with an average constant accuracy.

Ion preferences were determined for different ion binding sites. They were computed based on the fact that the relative preference of a site for two given ions can be measured by the ratio of the rate constants for the recognition of each individual ion. That is, if the rate constant for ion j is

$$R_j = N \exp(-\Delta G_j/kT),$$

where ΔGj is the free energy change between the ion in solution and bound, then the preference between ions i and j would be

$$p = R_i/R_j = \exp(-(\Delta G_i - \Delta G_j)/kT).$$

There is no direct way to compute the free energy changes ΔGi and ΔGj but it is possible to compute their difference. Consider the cycle represented by the free energy changes for the following transformations:

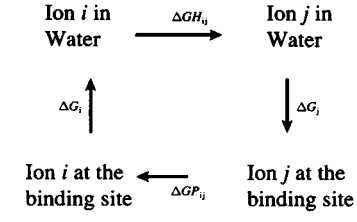

That is, two branches of the cycle represent the energy changes ΔGi and ΔGj, for moving ions between water and the binding site. The other two branches represent the energy changes $\Delta G_{H_{ij}}$ and $\Delta G_{P_{ij}}$, in trans-

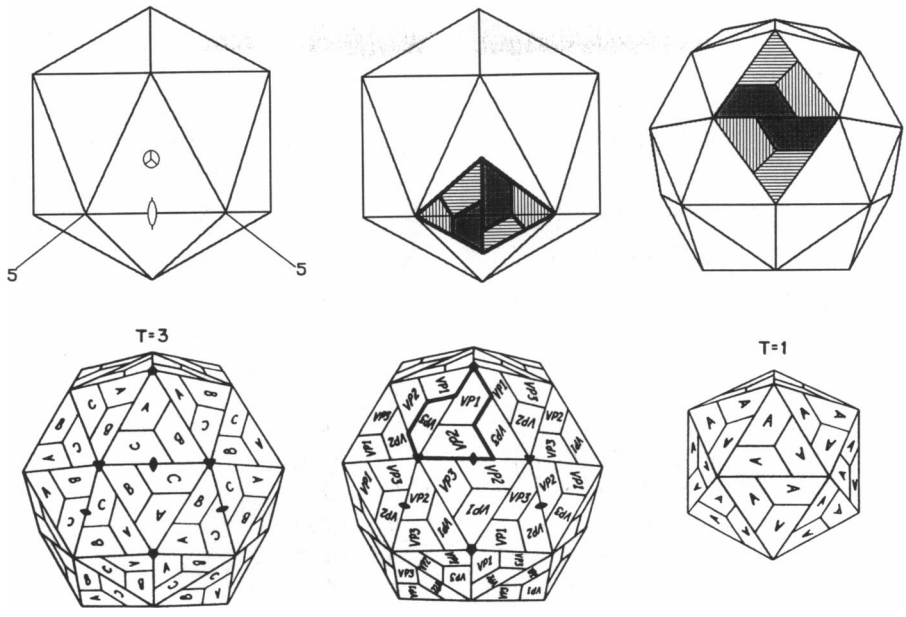

FIGURE 1 Schematic representation of the subunit packing in some icosahedral viruses. First row, from left to right: (*a*) the vertical icosahedral fivefold axis lies on the plane of the page. The symbols indicate the existence of symmetry axes. The circle with a triangular figure indicates the position of the threefold axis. One such axis is perpendicular to each face of the icosahedron. The elliptic symbol indicates the position of a twofold axis. The twofold axes lies on the middle point of each building line of the icosahedron. Finally, the number 5 and the line coming from the fivefold corners of the icosahedron indicates the presence of fivefold symmetry axes. (*b*) Typical disposition of three nonequivalent subunits and its twofold symmetry related images. By operating with the symmetry operators corresponding to the rotations described above the whole icosahedron will be covered with subunits. It is interesting to notice that only subunits with the vertical dash filling will surround the fivefold axis. Subunits with grey filling and horizontal dash filling will surround the threefold axis, defining a cuasi sixfold axis. Finally, only grey subunits surrounds the twofold symmetry axis. The most common perspective used for exploring the disposition of the subunits can be reached from *b* by rotating the figure around an axis perpendicular to the indicated twofold axis in the *a*, until this last twofold axis is perpendicular to the plane of the page. Then a rotation around this axis is applied (90° clockwise). After this rotation, (*c*) is obtained. The figures in the second row are presented from this perspective. (*d*) TBSV and SBMV are formed by 180 subunits, their triangulation number being $T = 3$. Since identical subunits, in terms of amino acid sequence, have to either form hexamers or pentamers, structural changes are required at different symmetry environments. Thus, three types of subunits are distinguished. Subunits *A* form pentamers at the fivefold axes and pairs of subunits *B* and *C* form hexamers around the threefold axes. (*e*) The picornavirus HRV14 and Mengovirus are formed by the icosahedral packing of 60 protomers, then the triangulation number of the capsid is $T = 1$. The protomers, built up by three surface proteins and a small internal one, exhibit some degree of internal symmetry such that they can be seen as pseudo $T = 3$ particles. The subunits VP1, VP2, and VP3 are at equivalent positions, respect to the symmetry axes, to those of subunits *A*, *B*, and *C*, respectively, in the $T = 3$ plant viruses. Subunit VP1 is by the fivefold axis but also the amino-terminals of VP3 and VP4 extend to that axis. (*f*) STNV capsid is formed by 60 subunits, all of them related by exact icosahedral symmetry. The triangulation number is $T = 1$.

forming one ion into another, either at the binding site or in water. Since these four free energy changes have to add to zero then

$$\Delta G_i - \Delta G_j = \Delta G_{H_{ij}} - \Delta G_{P_{ij}},$$

where $\Delta G_{H_{ij}}$ equals the difference in hydration energies, and $\Delta G_{P_{ij}}$ is the free energy change in transforming ion *i* into ion *j* within the binding site. $\Delta G_{H_{ij}}$ can be calculated since free energies for hydration are known for individual ions, Table 1. The computation of $\Delta G_{P_{ij}}$ can be performed using free energy perturbation methods (Beveridge and DiCapua, 1989), slowly varying the parameters defining a given atom into another during a molecular dynamics simulation. The molecular dynamics was restricted to allowing the movement of the ion, two water molecules at its sides and the amino acids forming the binding site. For instance, for SBMV only the movement of the fivefold related Thr 124, Thr 125, and Thr 126 was allowed, with Thr 124 and Thr 126 parabolically restrained to their starting, energy minimized, configurations. Typical molecular dynamics trajectories were 120 ps long. However, for HRV14 a 300 ps trajectory was computed for the transition K^+ to Ca^{++}. It should be noted that the derived relative preferences are to be seen as trends due to the limited flexibility imposed on the protein structures in order to reduce computing time for the dynamics. The preferences could be accurately quantified when the free movement of all amino acids building up the channel is allowed and when more water molecules are included in the molecular dynamics simulation, (Roux and Karplus, 1991).

Molecular dynamics calculations were performed on a CONVEX C220 computer (Convex Co., USA) at Johns Hopkins University (Baltimore, MD). Other calculations were performed at Bahia Blanca on a MicroVAX II computer (Digital Equipment Co., USA) using locally developed software. This mainly includes: a molecular graphics package running on a JUPITER J-Station (Jupiter Systems, Inc., USA); an accessibility surface program; and a program to add hydrogen atoms to the protein subunits, classify the atoms according to Clementi's nomenclature and add or subtract protons to the amino acid residues according to their pK and assumed pH of the medium (Kalko et al., 1991). Hydrogen atoms were added to the x-ray crystallographic structure coordinates following geometrical criteria and the orientation of H atoms by the symmetry axis were determined by energy minimization.

VIRAL STRUCTURES AROUND THE FIVEFOLD AXES AND THEIR BINDING SITES

The structures to be analyzed in each viral capsid were selected by taking all amino acids within 15 Å from the

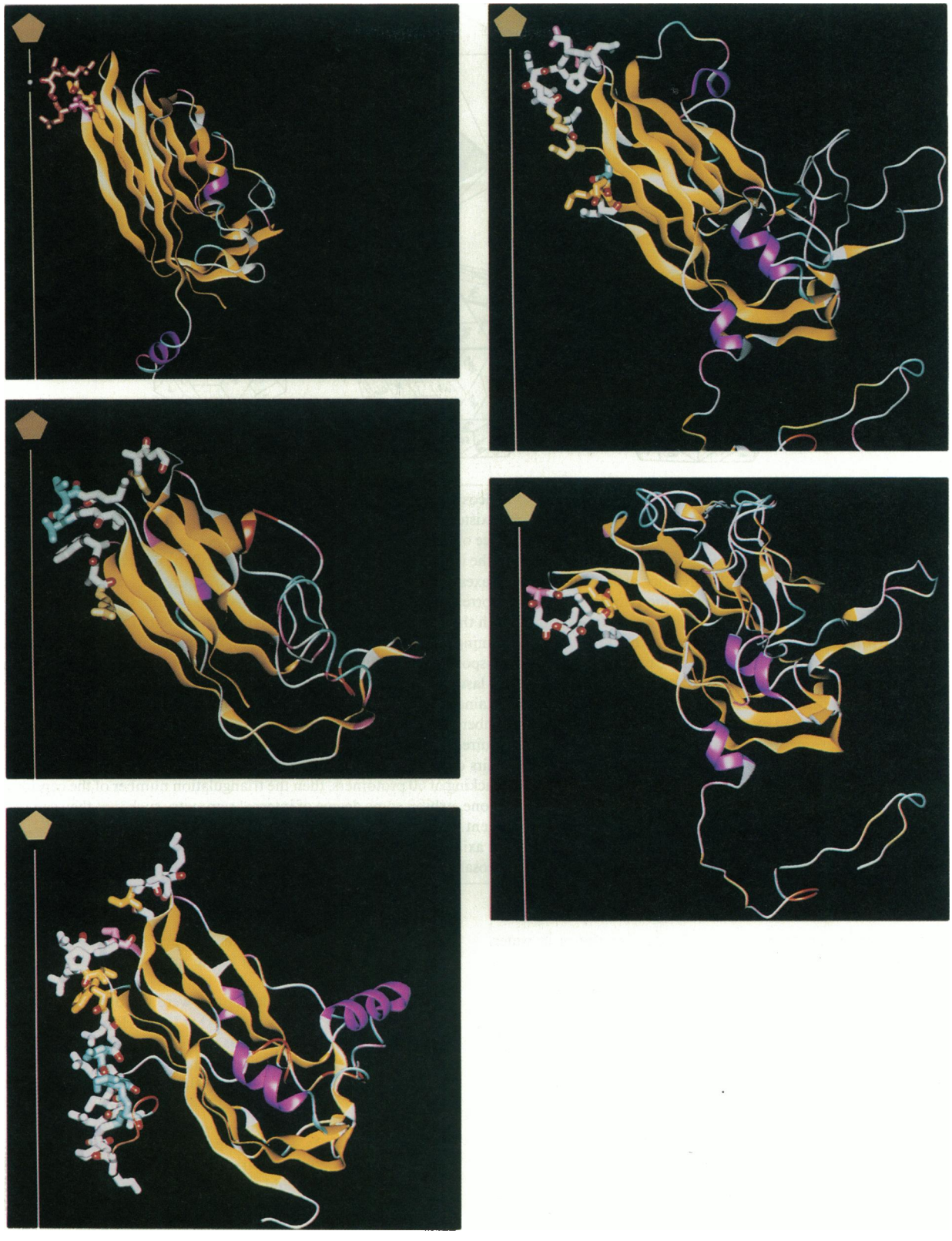

FIGURE 2 Ribbon model representations. The vertical lines indicate the direction of the fivefold axes. From top to bottom, and left to right: (*a*) STNV. (*b*) TBSV subunit *A*, shell domain. There is a second domain, not shown, extending from the carboxy terminal polypeptide laying on the external viral surface. (*c*) SBMV, subunit *A*. (*d*) HRV14, VP1. (*e*) Mengovirus, VP1.

TABLE 1 **Coordination chemistry for selected ions**

	Coord	OH	CO	Gh	P.R.
		Å	*Å*	*kcal/mol*	*Å*
Li	4	1.8 (0.1)			0.68
Li	6	2.0 (0.1)	2.1 (0.1)		
Na	5	2.4 (0.2)		−98.3	0.95
Na	7	2.5 (0.1)	2.6 (0.1)		
K	7	2.6 (0.2)	2.7 (0.1)	−80.8	1.33
Rb	8	2.9 (0.1)	3.0 (0.2)		1.48
Cs	7	3.1 (0.2)	3.2 (0.1)		1.69
Cs	8	3.2 (0.2)			
Mg	6	2.1 (0.1)	2.1 (0.1)	−455.5	0.65
Ca	6	2.3 (0.1)	2.4 (0.1)	−380.8	0.99
Sr	6	2.8 (0.1)	2.8 (0.1)		1.13
Ba	7	3.0 (0.2)	3.1 (0.2)		1.35
Ba	10	3.4 (0.1)	3.6 (0.2)		
Cl	6	3.5 (0.2)		−75.8	1.81
OH^-				−90.6	1.53
OH_3^+					1.14 (1.35)*
NH_4^+					1.48 (1.70)*

Coord: coordination number. CO: average distance from an ion to a chelating carbonyl oxygen. Computed after averaging data by Poonia and Bajaj (1985) and Izatt et al., (1985). OH: average distance from an ion to a chelating hydroxyl oxygen computed after averaging data by Poonia and Bajaj (1985) and Izatt et al., (1985). Gh: hydration free energy. P.R.: Pauling radii for ions. * Anisotropic radii as estimated from Fraga's pair potentials.

fivefold axis. Fig. 3 is a schematic representation of the virions, in relative scale, where a profile of the Na^+ accessibility surfaces for the structure included in the calculations have been displayed.

Tomato Bushy Stunt Virus (TBSV) and Southern Bean Mosaic Virus (SBMV)

TBSV was the first icosahedral virus whose structure was determined to 2.9-Å resolution (Harrison et al., 1978; Olson et al., 1983), but no refined coordinates of the molecular model are available. Nevertheless it is important to analyze the structure of TBSV due to its similarity with that of SBMV.

There is a remarkable structural homology between the SBMV protein subunit and the TBSV shell domain (Fig. 2, *a* and *b*). This similarity occurs despite the fact that their amino acid sequence homology is less than 20%. In other words, they have similar folding but very different side chains. Nevertheless, around the fivefold axis, at the narrowest section, both structures are virtually identical (Fig. 4). In TBSV this region is at the bottom of a short funnel-like structure lined by Glu 172, Asp 250 and some nonpolar residues from each subunit. In SBMV there is a more prominent funnel, lined by several polar residues (Fig. 5). Thus, at the external surfaces of both virions there is a well defined funnel built up by the fivefold repetition of loops connecting β-strands with an identical structure at the bottom. The conservation of these structures, involving ten threonines and five tryptophans, would in turn imply the conservation of ion selectivity properties. Moreover, amino acid sequence alignments suggest that the structural motif of threonines and tryptophans would also be present at the fivefold axis of Turnip Crinkle Virus.

A striking characteristic of the SBMV structure is its arrangement of amino acid residues around the fivefold axis that produces alternating rings of acidic and basic groups along the axis, Fig. 6 *c*. These side chains are contributed by a helix which is not present in TBSV, Figs. 2, *b* and *c*. However, TBSV has similar features since some basic and acidic residues emerge from the internal β-sheet facing the fivefold axis (Fig. 6 *b*). The electrostatic energy profiles computed along the fivefold axes suggest that both structures are adequate for ion transport (Figs. 7, *b* and *c*). Due to their high effective dipolar moment, the hydroxyl groups of the threonines near the axis are the main contributors to the energetics of ion-protein interactions in this region.

In contrast to what is observed in the case of the pentameric structures, the ion-protein interaction energies at the hexamers of both virions indicate that no ion could move along those axes. Only three polypeptide chains loop around the axis, making a compact structure of hydrophobic residues that exhibit exact threefold symmetry. Thus, the steric constraints in the hexamers preclude ion permeation.

Table 2 shows the distance from the oxygen hydroxyls of Thr 125 and Thr 170 in SBMV and TBSV, respectively, to the fivefold axes and to the minima of the interaction energy for different ions. A comparison with Table 1 suggests that in both cases the geometry of the site would favor the binding of Na ions. On the other hand, the free energy perturbation calculations for the transi-

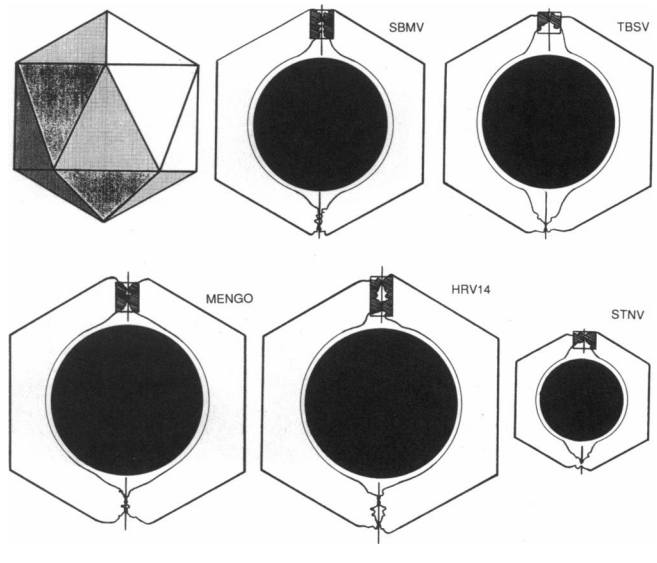

FIGURE 3 Schematic representation of viral protein coats. The shadowed regions are cuts of the accessibility surfaces for the atoms used in the calculations. Enlargements of each region are in Fig. 7.

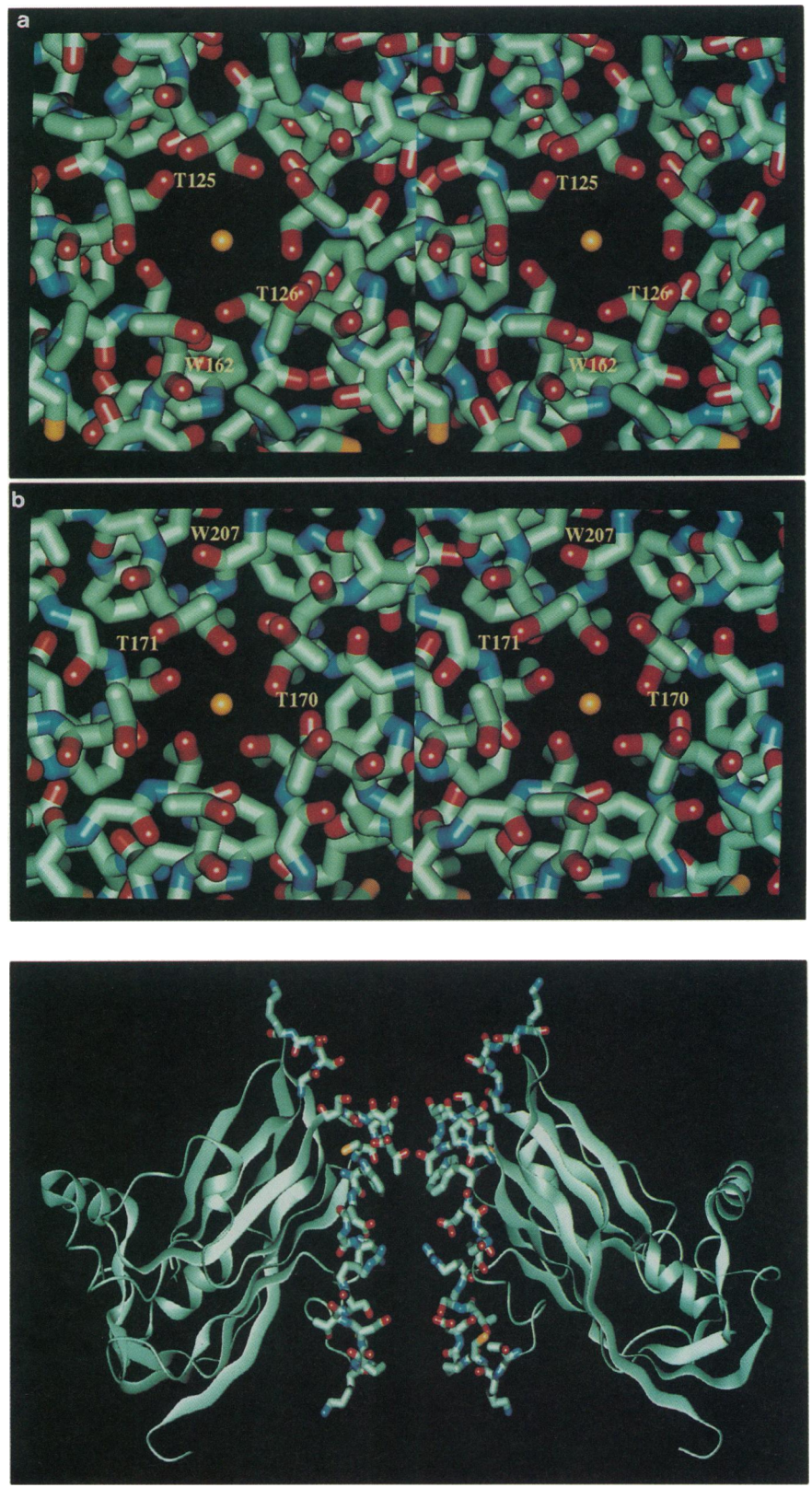

FIGURE 4 The narrowest sections of the channels in *a* SBMV and *b* TBSV. These structural motif are conserved despite the amino acid sequence homology between SBMV and TBSV is less than 20%. Amino acid sequence comparisons suggest that a similar structure is also present in turnip crinkle virus.

FIGURE 5 Ribbon model representation of two, out of five, subunits of SBMV around the fivefold axis. A funnel-shaped structure is formed by the fivefold association of the upper most loops which have Lys 234 at their tops. The fivefold axis is in the plane of the paper.

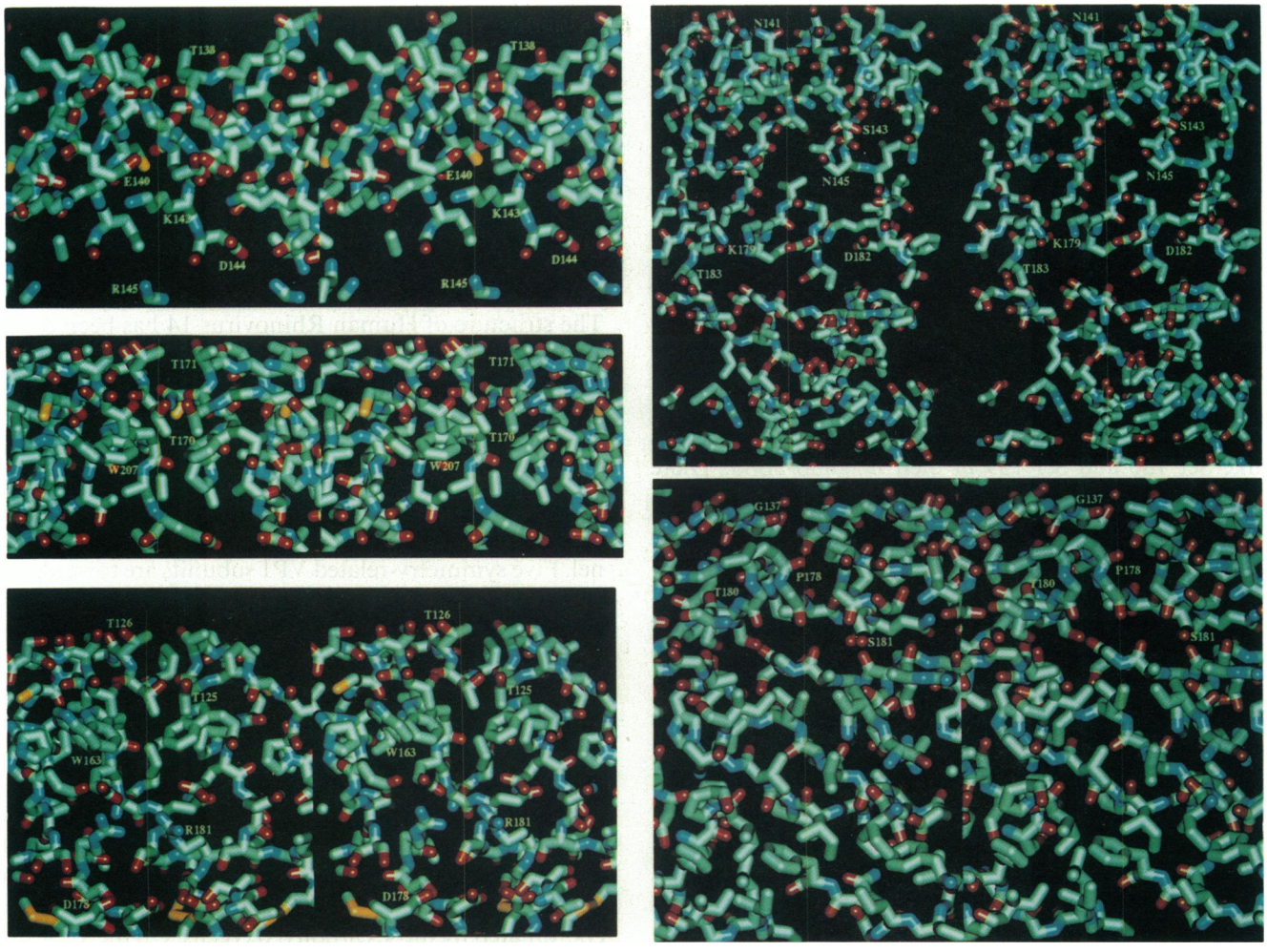

FIGURE 6 Stereoscopic projections of three out of five subunits around the fivefold axes, the axes laying on the plane of the paper. Only the residues by the axis are shown. From top to bottom and left to right: (*a*) STNV; (*b*) TBSV; (*c*) SBMV; (*d*) HRV14; (*e*) Mengovirus.

tions Na^+ to K^+ and K^+ to Cl^- suggest ion preferences Na > K ≫ Cl, Table 3. The dynamics were limited to allowing unrestricted movements of the threonines by the axis, the ion and two water molecules on the axis at both sides of the ion. The most favorable conformations of the threonines are different for each ion. For Cl^- and K^+ the hydroxyls are towards the external viral surface, while for Na^+ the side chains rotate around the CA—CB bond locating the hydroxyls towards the channel interior and the methyls in opposite direction.

Satellite Tobacco Necrosis Virus (STNV)

The structure of STNV has been determined and refined to 2.5 Å resolution (Liljas et al., 1982; Jones et al., 1984). Three metal ion sites have been identified in the protein coat, all of them postulated to be calcium ions (Unge et al., 1986). One ion is on the icosahedral threefold axes, another is in a general position and a third one is situated on the fivefold axis. The latter is coordinated by five carbonyl oxygens of the threonines 138 and two water molecules on the axis. STNV particles are known to contain calcium as well as magnesium ions (Liljas et al., 1982).

The fivefold related threonines 138, with their side chains on the viral external surface, form the narrowest

TABLE 2 Ion binding distances at the fivefold axis

	Rad.	Cl	Na	K
	Å	Å	Å	Å
STNV	2.1		2.5	2.9
TBSV	2.2	4.0	2.5	2.8
SBMV	2.2	4.0	2.5	2.9
HRV14 (carbonyls)	2.8		2.7	2.9
HRV14 (hydroxyls)	3.8	3.9	2.6*	2.7*
Mengovirus	3.7		2.7*	2.8*

Rad.: Distance from the carbonyl or hydroxyl oxygen forming the binding site to the fivefold axis. Cl, Na, K: Distance from the minimum for the potential energy interaction function on the fivefold axis for the ion to the coordinating atom. * Asymmetric minima, not on the fivefold axis.

TABLE 3 Ion preferences from FEPT calculations

STNV	$Na \overset{385.}{\gg} K \overset{1530.}{\gg} Cl$
TBSV	$Na \overset{47.}{>} K \overset{756.}{\gg} Cl$
SBMV	$Na \overset{71.}{>} K \overset{803.}{\gg} Cl$
HRV14 (carboxyls)	$Ca \overset{11.4}{>} Na \overset{1.7}{>} K \overset{2134.}{\gg} Cl$
HRV14 (hydroxyls)	$Cl \overset{178.}{>} K \overset{63.}{>} Na$
Mengo	$K \overset{115.}{>} Na \overset{1103.}{\gg} Cl$

Symbols between ions indicate the preference order at each binding site and the numbers indicate the magnitude of the relative preference.

section of the channel, Fig. 6 *a*. There are polar residues like Ser 136 and Ser 139 in their neighborhood. There are a few basic and acidic residues toward the virus interior, facing the axis, including Glu 140 and Lys 143, similar to the TBSV structure.

The electrostatic energy profile computed along the fivefold axis indicates that the structure is attractive for cations, Fig. 7 *a*. The major contributors to the energy minimum are the main chain carbonyl oxygens of the theronines 138. Although the structure is refined, the distance of 2.12 Å (Jones et al., 1984) from the carbonyl oxygens to the axis seems too short for a calcium ion binding site.

The interaction energy calculations at the threefold axis show high steric barriers for all ions, thus, no ion could move along this axis. The ion found on the threefold axis is coordinated by OD2 of Asp 55 and is deeply buried in the protein coat. The distance of 1.4 Å (Jones et al., 1984) from the coordinating OD2 to the calcium ion seems too short for binding.

Comparing the coordination distances for the carbonyl binding site of Thr 138 with the standard coordination distances, Tables 1 and 2, it becomes apparent that the bound cation should be a magnesium ion. Moreover, since the virion was crystallized in a 0.001 M magnesium sulfate solution (Lentz et al., 1976), it would not be unlikely to find a magnesium ion at the site. It should also be kept in mind that the virions in solution do contain magnesium ions (Liljas et al., 1982). It has been reported that in swelling experiments where a virus solution is incubated with EDTA, the cation at the fivefold axis is the last ion to be released from the capsid (Unge et al., 1986). This observation further supports the proposal that a magnesium ion is located at the fivefold axis, since the equilibrium constants for the Mg-EDTA chelate and the Ca-EDTA chelate differ by two orders of magnitude, (Log K(Mg-EDTA) = 8.69 and Log K(Ca-EDTA) = 10.7), (Fisher et al., 1969). This means that all Ca ions would be released before the Mg ions start to be released from the capsid. This preference is increased in these experiments since the EDTA solution includes magnesium sulfate in order to prevent the hydrolysis of the RNA in the expanded virus particle.

The free energy perturbation calculations were computed similarly to the SBMV and TBSV ones. In this case unrestrained movements of Thr 138, the ion and two waters were allowed. The calculation suggests a preference for Na ions, Table 3. A transition including a Mg ion could not be computed since pair potential parameters are not available for the ion, as was already discussed in Methods.

Human Rhinovirus 14 (HRV14)

The structure of Human Rhinovirus 14 has been determined and refined with x-ray diffraction data extending to 3.0 Å resolution (Rossmann et al., 1985; Arnold et al., 1990).

In the $T = 3$ plant viruses the fivefold channel is formed by interactions of only one type of subunit. In the case of HRV14 there are three different subunits, related by fivefold symmetry, creating a 40-Å long channel. Five symmetry-related VP1 subunits are towards the external viral surface; next along the axis are the amino-terminal polypeptides of VP3 subunits and further inside there are polypeptides of VP4. In general terms the fivefold channel can be described as a wide cavity, populated by several water molecules, with narrow ends towards the external and internal protein coat surfaces (Fig. 7 *e*). On the VP1 side the narrowest section is very close to the external surface and it is formed by fivefold related carbonyl oxygens from asparagines 141 which are 2.92 Å away from the axis (Fig. 6 *d*). The electron density map indicates the presence of an ion on the axis coordinated by those carbonyl oxygens. On the viral surface surrounding the entrance of the channel, there is a cluster of charges including the following amino acids from VP1: Glu 231, His 232, Asp 233, Glu 234, His 235, and Lys 236. From Asn 141 towards the virion interior, the channel widens and there are several polar and charged residues from VP1 facing the axis, including Ser 143, Asn 145, Lys 179, and Asp 182 (Fig. 6 *d*).

The inner narrow section is formed by a β-cylinder: a fascinating structure built up by the fivefold twisting of hydrogen bonded amino terminal strands of VP3. There are several polar residues by the axis with threonines 4 making the closest approach to the axis in a conformation similar to that observed for Thr 125 of SBMV and Thr 170 of TBSV. There is also an electron density maximum on the axis near the hydroxyl groups of the threonines 4.

The electrostatic energy profile (Fig. 7 *e*) indicates that the structure is attractive for cations from the external viral surface, with a minimum at the VP1 Asn 141 binding site. In contrast, the region by VP3 Thr 4 is more favorable for interaction with anions.

The external binding site created by Asn 141 carbonyls has been postulated to be a site for calcium (Smith et al., 1986). Nevertheless, the geometry of the site agrees better with a potassium ion than with a calcium ion (Tables 1 and 2). Note that since both ions are isoelectronic,

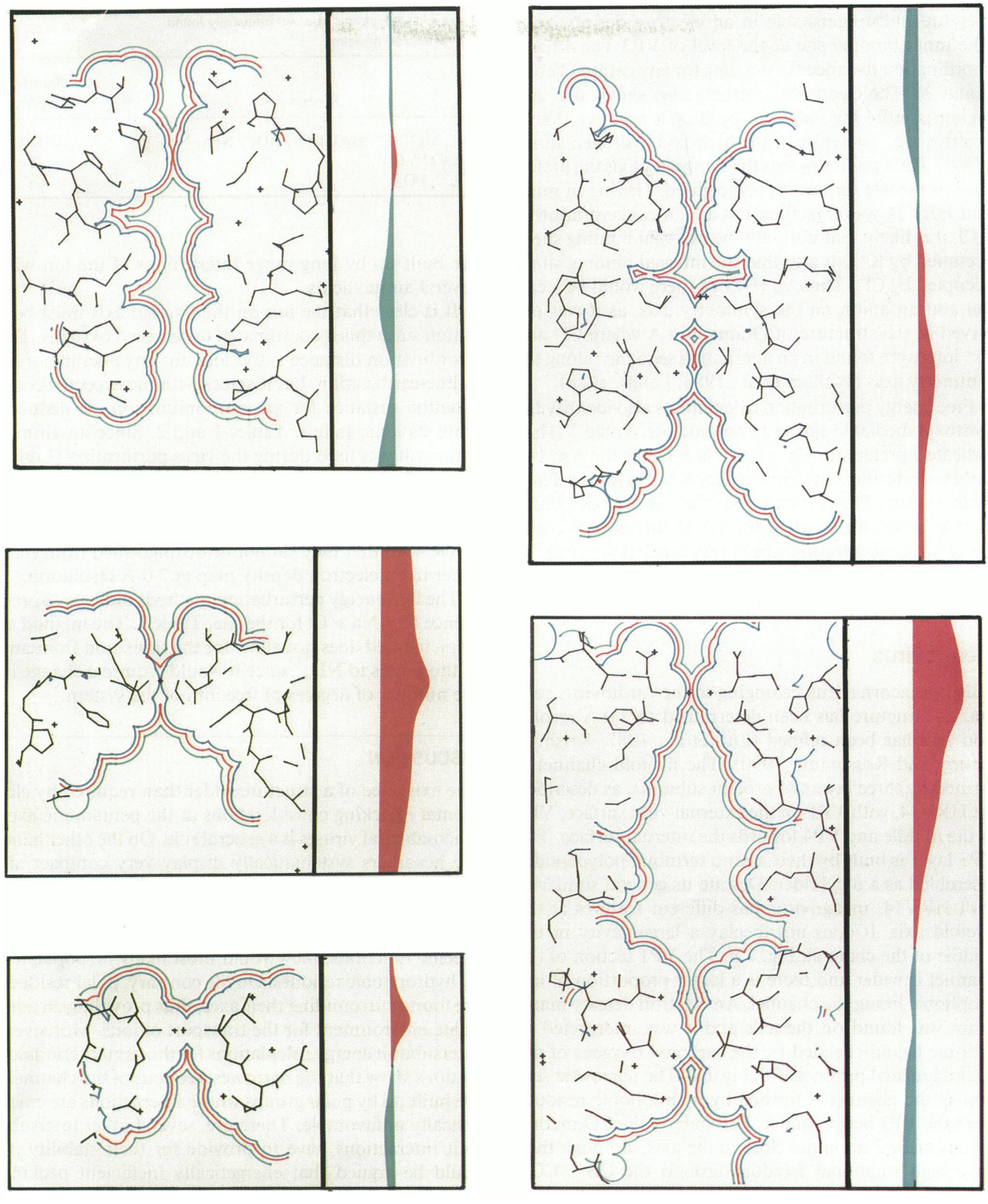

FIGURE 7 Accessibility and electrostatic energy profiles. The accessibility profiles correspond to Na^+, Cl^- and K^+ represented in blue, red, and green, respectively. The electrostatic energy profiles on the axis were computed using the coulombic term of Fraga's potential. The energy axis extends from −100 to +100 kcal/mol. Regions in red are attractive for cations and regions in blue are attractive for anions. Clockwise from left bottom corner (*a*) STNV; (*b*) TBSV; (*c*) SBMV; (*d*) Mengovirus; (*e*) HRV14.

they are indistinguishable in an electron density map. The inner binding site at the level of VP3 Thr 4 has a coordination distance far too long for any cation (Tables 1 and 2). The electrostatic profile also shows that this region is more favorable for binding a negative than a positive ion. Therefore, if the hydroxyl hydrogen atoms of VP3 Thr 4 point towards the symmetry axis the preference of the site for anions is increased. Having in mind that HRV14 was crystallized at a high concentration of KCl, it is likely that not only the external binding site is occupied by K^+ but also that the internal binding site is occupied by Cl^-. Thus, in HRV14 there would be a cation and an anion on the symmetry axis, as it was observed in the structure of Gramicidin A where Cl^- and Cs^+ ions were found in an alternating sequence along the symmetry axes (Wallace et al., 1988; Langs, 1988).

Free energy perturbation calculations also identify the hydroxyl mediated site as an anionic site, Table 3. They indicate a preference Ca > K > Na ≫ Cl for the Asn 141 carbonyl site and a preference Cl > K > Na for the Thr 4 hydroxyl site. The preference for Ca^{++} is only one order of magnitude higher than for K^+ at the carbonyl site. Thus, ion concentration would very much determine the type of ion bond. This site is analyzed in depth in a following article.

Mengovirus

This is a picornavirus belonging to the cardiovirus genera. Its structure has been determined to 3.0-Å resolution and has been refined (Luo et al., 1987; Krishnaswamy and Rossmann, 1990). The fivefold channel is formed by three layers of protein subunits, as described for HRV14, with VP1 on the external viral surface, VP3 in the middle and VP4 towards the internal surface. The VP3 layer is built by their amino terminal polypeptides assembled as a β-cylinder. Despite its general similarity with HRV14, mengovirus has different features at the fivefold axis. It does not display a large cavity in the middle of the channel, Fig. 7 *d*. The VP1 section of the channel is wider and there is a larger proportion of hydrophobic lining the channel. An electron density maximum was found on the axis and it was interpreted as cationic ligand chelated by the carbonyl oxygens of the fivefold related prolines 178, Fig. 6 *e*. The narrowest section of the channel is formed by hydrophobic residues from the VP3 beta cylinder. Particularly the CD methyl groups of Ile 7 are quite close to the axis, although they have high rotational freedom around the CB—CG1 bond.

As expected for a very wide structure the electrostatic profile on the fivefold axis evolves smoothly, Fig. 7 *d*, and a well defined minima at the Pro 178 site is not observed. The general pattern of this profile shows that the structure is adequate for the transport of ions, specially for cations. The repulsive regions of the channel are not contributed by any specific residue, rather, they are built up by long range interactions of the ion with several amino acids.

TABLE 4 **Isoelectronic species frequently found in crystallized proteins**

Species	Number of electrons
Na^+, Mg^{++}, F^-, H_2O, HO^-, HO_3^+, NH_3, NH_4^+	10
K^+, Ca^{++}, Cl^-	18
SO_4^{--}, PO_4^{---}	48

It is clear that the ion on the fivefold axis must be a cation since this is coordinated to carbonyl oxygens. The coordination distance is too long for any alkaline or alkaline-earth cation, but it agrees with the expected coordination distance for an ammonium ion, as deduced from its ionic radius, Tables 1 and 2. Since an ammonium salt was used during the virus purification (Luo et al., 1987; Boege et al., 1984), it seems reasonable to assume that the cation is an ammonium ion. It has to be noticed that NH_4^+ is isoelectronic with respect to water, Table 4, so that they cannot be distinguished from each other in an electron density map at 3.0-Å resolution.

The free energy perturbation methods indicates a preference K > Na ≫ Cl for the site, Table 3. The method as implemented does not allow for the transition from any of those ions to NH_4^+ since it would require a change in the number of degrees of freedom of the system.

DISCUSSION

The existence of a structure wider than required by elementary packing considerations at the pentameric axes of icosahedral viruses is a general rule. On the other hand the hexamers systematically display very compact arrangements of hydrophobic amino acids by their axes. Thus, if the fivefold viral channels were just the consequence of subunit packing and steric constraints with no specific functions, they would most likely be populated by hydrophobic residues. On the contrary, polar residues are found surrounding their axes, thus providing an adequate environment for the transport of ions. Moreover, intersubunit energy calculations for the pentameric associations show that the narrowest sections of the channels are built up by polar groups whose interactions are energetically unfavorable. Therefore, several other intersubunit interactions have to provide for their stability. It could be argued that energetically inefficient packing would not exist but with a specific function.

The viral channels have well defined funnels at their entrances in some cases, but most important, they have ion binding sites. The sites are either carboxyl- or hydroxyl-oxygen mediated. Contrary to what might be expected, acidic or basic side chains play no direct role in binding. Rather, short range dipolar interactions give rise to localized binding sites. Carbonyl sites can bind

only cations due to the negative partial charge associated to the oxygens but hydroxyls can participate in binding either cations or anions depending upon the orientation of their associated dipoles. The dual character of dipole-mediated sites is not a new concept. In fact, this is the basic principle behind the dissolution of salts in water. This duality is clearly displayed in Table 1, which shows the average coordination distances of selected ions with carbonyl and hydroxyl oxygens. Note also that the ion identity is unambiguously defined by the coordination distance.

The evidence presented in this work suggest that the ions at the sites, in all cases, correspond to ions in the crystallization or purification buffers. Thus there would be an actual transport of ions from the external media to, at least, the binding site which requires the dehydration of the ion.

To summarize, these channel-like structures have the features expected for functional ion channels: a polar internal environment with frequently alternating acidic and basic residues, ion binding sites, the capability to induce ion dehydration, ion transport from the external viral surface to the binding sites and in some cases a funnel at their entrances.

There are other icosahedral viruses whose structures have been determined but have not been analyzed in this work. The reports describing those structure and the atomic models, when their coordinates are available, all seem to support the ion channel hypothesis. The structure of Foot-and-Mouth Disease Virus shows wide channels at the fivefold axes and the authors proposed these channels as the Cs^+ ions entrance pathway to the virion (Acharya et al., 1989). The bacterial virus MS2, (Valegard et al., 1990), is very different from any other icosahedral virus. The authors report a hole of 17 Å diameter at the hexamers and a cylindrical channel 14 Å in length and 16 Å in diameter at pentamers. Canine Parvovirus has a cylindrical structure around its fivefold axis lined by small hydrophilic residues. The smallest diameter is 8 Å. Inside this wide structure there is electron density extending along the axis for about 17 Å, which the authors propose to be part of the polypeptide of VP2 or VP3, (Tsao et al., 1991).

In poliovirus, (Hogle et al., 1985), there are polar groups by the fivefold axis and a possible binding site created by a packed array of fivefold related His 149 from VP1. The narrowest section of the fivefold channel in Bean-Pod Mottle Virus (Chen et al., 1989) is formed by Ser 85 of subunit S, which is surrounded by several basic and acidic amino acids. In Human Rhinovirus 1A, (Kim et al., 1989), there is Asp 136 from VP1 very close to the fivefold axis and several acidic and basic amino acids in its neighborhood.

On the experimental side there are some indirect evidences of capsid permeability to ions. The variations of virion density in Cs^+ salt gradients is frequently observed in icosahedral viruses, including SBMV and FMDV (Rowlands et al., 1971; Hull, 1977). These measurements suggest that the virion protein coat is permeable to Cs^+, but they cannot exclude permeability to lighter ions since they would produce nondetectable density changes. Durham et al. (1984) observed hysteresis effects in hydrogen-ion titration experiments on several plant viruses solutions, which lead him to propose the existence of some type of channels across the protein coat.

There are also a series of experiments showing that picornaviruses induce changes in the cell membrane permeability during virus entry (Carrasco, 1981) and at the stage of viral protein synthesis, (Carrasco, 1978; Contreras and Carrasco, 1979). An increase of the cell permeability to monovalent ions is observed, from the third hour post-infection, when HeLa cells are infected by poliovirus, (Lopez-Rivas et al., 1987). The collapse of monovalent cations gradients has been correlated with the shut-off of cellular functions, (Castrillo et al., 1987).

All viruses that we have examined display rich polar environments around their fivefold axes, with no exceptions. Some of them look like text-book examples of what protein ion-channels are supposed to be. About their functional roles, it would be tempting to speculate that they relate to the permeability changes of cell membranes induced by viral infections. Nevertheless it is clear that through those channels the inner viral media would be sensitive to external ion concentration changes and then to its environment. Thus, the channels might work as sensors that would trigger specific viral processes.

We wish to thank Professor Michael G. Rossmann for sending us the refined coordinates of HRV14 and Mengovirus and Professor Mario Amzel for his active support. We also thank Marcelo Yezzi and Sandra Gabelli for the development of the molecular graphics package, and Captain E. Secchi for lending us part of the computer graphics hardware. We thank D. M. A. Guerin for his critical reading of the manuscript.

We also wish to thank Dr. John W. Erickson for his support for the conclusion of this work. Research was supported in part by the National Cancer Institute, DHHS, under contract NO1CO-74102 with Program Resources, Incorporated. The contents of this publication do not necessarily reflect the views or policies of the DHHS, nor does mention of trade names, commercial products, or organizations imply endorsement by the United States government.

This work was made possible by a grant from the Secretaria de Ciencia y Tecnica de la Republica Argentina to AMS, and a fellowship given to SGK by the Comision de Investigaciones Cientificas de la provincia de Buenos Aires.

Received for publication 25 July 1990 and in final form 3 April 1992.

REFERENCES

Abad-Zapatero, C., S. S. Abdel-Meguid, J. E. Johnson, A. G. W. Leslie, I. Rayment, M. G. Rossmann, D. Suck, and T. Tsukihara. 1980. Structure of southern bean mosaic virus at 2.8 Å resolution. *Nature (Lond.)*. 286:33–39.

Acharya, R., E. Fry, D. Stuart, G. Fox, D. Rowlands, and F. Brown. 1989. The three-dimensional structure of foot-and-mouth disease virus at 2.9 Å resolution. *Nature (Lond.).* 337:709–716.

Arnold, E., and M. G. Rossmann. 1990. Analysis of the structure of a common cold virus, human rhinovirus 14, refined at a resolution of 3.0 E. *J. Mol. Biol.* 211:763–801.

Benoit, R., and M. Karplus. 1991. Ion transport in a model gramicidin channel: structure and thermodynamics. *Biophys. J.* 59:961–981.

Beveridge, D. L., and F. M. Di Capua. 1989. Free energy via molecular simulation: A Primer. Computer simulation of biomolecular systems. W. F. van Gunsteren and P. K. Weiner, editors. ESCOM Science Publishers B.V., Leiden, The Netherlands.

Bidacovich, E. A., S. G. Kalko, and R. E. Cachau. 1990. GAMYR: a generalized version of AMYR for the study of biomolecules. *J. Mol. Str. (Theochem.).* 210:455–465.

Boege, U., D. G. Scraba, K. Hayakawa, M. N. G. James, and J. W. Erickson. 1984. Structure of the mengo virion VII. Crystallization and preliminary x-ray diffraction analysis. *Virology.* 138:162–167.

Cachau, R. E., E. H. Serpersu, A. S. Mildvan, J. T. August, and L. M. Amzel. 1990. Recognition in cell adhesion. A comparative study of the conformation of RGD-containing peptides by Monte Carlo and NMR methods. *J. Mol. Recogn.* 2:179–186.

Carrasco, L. 1978. Membrane leakiness after viral infection and a new approach to the development of antiviral agents. *Nature (Lond.).* 272:694–699.

Carrasco, L. 1981. Modification of membrane permeability induced by animal viruses early in infection. *Virology.* 113:623–629.

Caspar, D., and A. Klug. 1962. *Cold Spring Harbor Symp. Quant. Biol.* 27:1–24.

Castrillo, J. L., A. Lopez-Rivas, and L. Carrasco. 1987. Effects of extracellular cations on translation in poliovirus-infected cells. *J. Gen. Virol.* 68:325–333.

Chen, Z., Y. L. Stauffacher, T. Schmidt, W. Bomu, G. Kamer, M. Shanks, G. Lomonossoff, and J. E. Johnson. 1989. Protein-RNA interactions in an icosahedral virus at 3.0 Å resolution. *Science (Wash. DC).* 245:145–159.

Clementi, E. 1980. Computational aspects of large chemical systems. *Lecture Notes in Chemistry 19.* Springer Verlag, Berlin.

Contreras, A., and L. Carrasco. 1979. Selective inhibition of protein synthesis in virus-infected mammalian cells. *J. of Virol.* 29:114–122.

Corongiu, G., and E. Clementi. 1978. Study of the structure of molecular complexes. XVI. Doubly charged cations interacting with water. *J. Chem. Phys.* 69:4885–4887.

Durham, A. C. H., J. Witz, and J. B. Bancroft. 1984. The semipermeability of Simple Spherical Virus Capsids. *Virology,* 131:1–8.

Eisenman, G., and O. Alvarez. 1991. Structure and function of channels and channelogs as studied by computational chemistry. *J. Membr. Biol.* 119:109–132.

Eisenman, G., A. Oberhauser, and F. Benzanilla. 1988. Ion selectivity and molecular structure of binding sites and channels in icosahedral viruses. Transport Through Membranes: Carriers, Channels and Pumps. A. Pullman et al., editors. Kluwer Academic Publishers, The Netherlands. 27–50.

Eisenman, G., and A. Villaroel. 1988. Ion selectivity of pentameric protein channels: backbone carbonyl ligands as cation binding ligands and side chain hydroxyls as "ambidextrous" ligands for cations or anions in viral capsids. *In* Monovalent Cations in Biological Systems. C. A. Pasternak, editor. CRC Press Publishers, Boca Raton, FL.

Erickson, J. W., A. M. Silva, M. R. N. Murthy, I. Fita, and M. G. Rossmann. 1985. The structure of a T = 1 icosahedral empty particle from Southern Bean Mosaic Virus. *Science (Wash. DC).* 229:625–629.

Fisher B., and D. G. Peters. 1969. A Brief Introduction to Quantitative Chemical Analysis. W. B. Saunders, Philadelphia.

Fraga, S. 1982. Molecular associations and reactions. *In* Current Aspects of Quantum Chemistry. Elsevier Publishing Co., Amsterdam.

Gelin, B. R., and M. Karplus. 1979. Side-chain torsional potentials: effect of dipeptide, protein and solvent environment. *Biochemistry.* 79:1256–1260.

Harrison, S. C., A. J. Olson, C. E. Schutt, F. K. Winkler, and G. Bricogne. 1978. Tomato bush stunt virus at 2.8 Å resolution. *Nature (Lond.).* 276:386–373.

Hogle, J. M., A. Maeda, and S. C. Harrison. 1986. Structure and assembly of turnip crinkle virus. I. X-ray crystallographic analysis at 3.2 Å resolution. *J. Mol. Biol.* 191:625–638.

Hosur, M. V., R. C. Schmidt, J. E. Johnson, T. M. Gallagher, B. H. Selling, and R. R. Rueckert. 1987. Structure of an insect virus at 3.0 Å resultion. *Proteins.* 2:167–176.

Hull, R. 1977. The banding behavior of viruses of the southern bean mosaic virus group in gradients of ceasium sulphate. *Virology.* 79:50–57.

Izatt, R. M., J. S. Bradshaw, S. A. Nielsen, J. D. Lamb, and J. J. Christensen. 1985. Thermodynamics and kinetics for cation-macrocycle interaction. *Chem. Rev.* 85:271–339.

Jones, T. A., and L. Liljas. 1984. Structure of satellite tobacco necrosis virus after crystallographic refinement at 2.5 Å resolution. *J. Mol. Biol.* 177:735–767.

Kim, S., T. J. Smith, M. S. Chapman, M. G. Rossmann, D. Pevear, F. J. Dutko, P. J. Felock, G. D. Diana, and M. A. McKinlay. 1989. Crystal structure of Human Rhinovirus serotype 1A. *J. Mol. Biol.,* 210:91.

Kistenmacher, H., H. Popkie, and E. Clementi. 1974. Study of the structure of molecular complexes. VIII. Small clusters of water molecules surrounding Li^+, Na^+, K^+, F^- and Cl^- ions. *J. Chem. Phys.* 61:799–814.

Krishnaswamy, S., and M. G. Rossmann. 1990. Structural Refinement and Analysis of Mengo Virus. *J. Mol. Biol.* 211:803–844.

Langs, D. A. 1988. Three-dimensional structure at 0.86 Å of the uncomplexed form of the transmembrane ion channel peptide gramicidin A. *Science (Wash. DC).* 241:188–191.

Lentz, P. J., B. Strandberg, T. Unge, I. Vaara, A. Borell, K. Fridborg, and G. Petef. 1976. The determination of the heavy-atom substitution sites in the satellite tobacco necrosis virus. *Acta Cryst.* B32:2979–2983.

Liddington, R. C., Y. Yan, J. Moulai, R. Sahli, T. L. Benjamin, and S. C. Harrison. 1991. Structure of simian virus 40 at 3.8 Å resolution. *Nature (Lond.).* 354:278–284.

Liljas, L., T. Unge, T. A. Jones, K. Fridborg, S. Lovgren, U. Skoglund, and B. Strandberg. 1982. Structure of satellite tobacco necrosis virus at 3.0 Å resolution. *J. Mol. Biol.* 159:93–108.

Lopez-Rivas, A., J. L. Castrillo, and L. Carrasco. 1987. Cation content in poliovirus-infected HeLa cells. *J. Gen. Virol.* 68:335–342.

Luo, M., G. Vried, G. Kamer, I. Minor, E. Arnold, M. G. Rossmann, U. Boege, D. G. Scraba, G. M. Duke, and A. C. Palmenberg. 1987. The atomic structure of mengo virus at 3 Å resolution. *Science (Wash. DC).* 235:182–191.

Nilar, S. H., and S. Fraga: 1984. Molecular associations: values of the expansion parameters for new classes of atoms. *J. Comp. Chem.* 5:261–262.

O'Donnell, T. J., and A. J. Olson. 1981. GRAMPS: a graphics language for real-time, interactive, three-dimensional picture editing and animation. *Computer Graphics.* 15:133–141.

Olson, A. J., G. Bricogne, and S. C. Harrison. 1983. Structure of tomato bushy stunt virus IV. The virus particle at 2.9 E resolution. *J. Mol. Biol.* 171:61–93.

Pflugrath, J. W., and F. A. Quiocho. 1985. Sulphate sequestred in the sulphate-binding protein of Salmonella typhimurium is bound solely by hydrogen bonds. *Nature (Lond.).* 314:257–260.

Poonia, N. S., and A. V. Bajaj. 1979. Coordination chemistry of alkali and alkaline earth cations. *Chem. Rev.* 79:389–445.

Rossmann, M. G., C. Abad-Zapatero, M. A. Hermodson, and J. W. Erickson. 1983. Subunit interactions in southern bean mosaic virus. *J. Mol. Biol.* 166:37–83.

Rossmann, M. G., E. Arnold, J. W. Erickson, E. A. Frankenberger, J. P. Griffith, H. J. Hecht, J. E. Johnson, G. Kamer, M. Luo, A. G. Mosser, R. R. Rueckert, B. Sherry, and G. Vriend. 1985. The structure of a human common cold virus (Rhinovirus 14) and its functional relations to other picornaviruses. *Nature (Lond.)*, 317:45–153.

Rowlands, D. J., D. V. Sangar, and F. Brown. 1971. Bouyant density of picornaviruses in ceasium salts. *J. Gen. Virol.* 13:141–142.

Silva, A. M., R. E. Cachau, and D. Goldstein. 1987. Ion channels in southern bean mosaic virus capsid. *Biophys. J.* 52:595–602.

Silva, A. M., and M. G. Rossmann. 1987. The refined structure of Southern Bean Mosaic Virus at 2.8 Å resolution. *J. Mol. Biol.* 197:69–87.

Silva, A. M., and M. G. Rossmann. 1985. The refinement of southern bean mosaic virus in reciprocal space. *Acta Crystallogr.* B41:147–157.

Smith, T. J., M. J. Kremer, M. Luo, G. Vriend, E. Arnold, G. Kamer, M. G. Rossmann, M. A. McKinlay, G. D. Diana, and M. J. Otto. 1986. The Site of Attachment in Human Rhinovirus 14 for Antiviral Agents that Inhibit Uncoating. *Science (Wash. DC).* 233:1233–1356.

Snow, M. E., and L. M. Amzel. 1986. Calculating Three-Dimensional Changes in Protein Structure due to Amino-Acid Substitutions: The variable Region of Immunoglobulins. *Proteins.* 1:267–279.

Stroud, R. M., M. P. McCarthy, and M. Shuster. 1990. Nicotinic acetylcholine receptor superfamily of ligand-gated ion channels. *Biochemistry.* 29:1109–11023.

Tsao, J., S. Chapman, M. Agbandje, W. Keller, K. Smith, H. Wu, M. Luo, T. J. Smith, M. G. Rossmann, R. W. Compans, and C. R. Parrish. 1991. The three dimensional structure of canine parvovirus and its functional implications. *Science (Wash. DC).* 251:1456–1464.

Unge, T., I. Montelius, L. Liljas, and L. Ofverstedt. 1986. The EDTA-Treated Expanded Satellite Tobacco Necrosis Virus: Biochemical Properties and Crystallization. *Virology.* 152:207–218.

Valegard, K., L. Liljas, K. Fridborg, and T. Unge. 1990. The three-dimensional Structure of the bacterial virus MS2. *Nature (Lond.).* 345:36–41.

Wallace, B. A., and K. Ravikumar. 1988. The gramicidin pore: crystal structure of a cesium complex. *Science (Wash. DC).* 241:182–187.

Woodward, W. 1968. Ionic Crystals, Lattice Defects and Nonstoichiometry. Butterworth and Co., Ltd., London.

Young, E. F., E. Ralston, J. Blake, J. Ramachandran, Z. W. Hall, and R. M. Stroud. 1985. Topological mapping of the acetylcholine receptor: evidence for a model with five transmembrane segments and a cytoplasmatic COOH-terminal peptide. *Proc. Natl. Acad. Sci. USA.* 82:626–630.